

Neighbor-Constrained Active Contours Without Edges

Hongda Mao¹,Huafeng Liu¹, and Pengcheng Shi²

¹State Key Laboratory of Modern Optical Instrumentation
Zhejiang University, Hangzhou, China

²College of Computing and Information Sciences, Rochester Institute of Technology

Abstract

To achieve robustness against different images, a novel region-based geometric deformable model framework employing neighboring information constraints is proposed. The fundamental power of this strategy makes uses of the image information at the support domain around each point of interest, thus effectively enlarges the capture range of each point to have a better regional understanding of the information within its local neighborhood. In other words, we establish the Mumford-Shah energy functional on each image point with its local neighborhood in a way such that it is capable of providing sufficient information to define a desired segmentation which is robust against intensity inhomogeneity and noise impact. The resulting partial differential equation is solved numerically by the finite differences schemes on pixel-by-pixel domain. Experimental results on synthetic and real images demonstrate its superior performance.

1. Introduction

It has been the fundamental goal of many efforts in computer vision community to identify regions with similar patterns in images. Approaches to this segmentation problem typically fall into two groups. The first one formulates as an energy minimizing contour with smoothness constraints deformed according to image data, including notable parametric active contour model [4]and geometric active contour model[1, 7]. One attractive feature of geometric active contour is that it can naturally handle changes in topology of the evolving contour.

The second group attempts to find object boundaries using region-based approaches based on level sets method, offering efficient alternatives to the edge-based algorithms for active contours[2, 10, 11]. These region-based geometric deformable models have received a large amount of attention in recent years. The major advantages of using the

region-based approaches over edges-based methods include the following. First, with this scheme, it does not use the gradient to detect boundaries, which allows it to segment color and multi-spectral images where there are no clear gradient-boundaries. Second, these region-based models are less sensitive to the location of the initial contours. Finally, these models have better ability to capture concavities of objects and less sensitive to noise. The most celebrating region-based model was introduced by Mumford and Shah[8], the model is designed to both extract the boundary of distinct regions while smoothing the image within these regions. Inspired by the basic idea of the Mumford-Shah model, in [2],Chan and Vese reduced the model into piecewise constant Mumford-Shah model, and solved it in the framework of level set. The piecewise constant Mumford-Shah model has been one of the most popular region-based segmentation strategies in recent years.

Even though piecewise constant Mumford-Shah models are very promising, these algorithms still have certain drawbacks. The serious drawback of the algorithm is its lacking the ability to deal with images of intensity inhomogeneity, since they assume that an image consists of statistically homogeneous regions. Secondly, they may be sensitive to local minima in the noisy images. However,intensity inhomogeneous is very common in real images, especially among biomedical images.

In order to overcome these problems and achieve robustness against varying imaging conditions, several new models have been developed and successfully applied to image segmentation. In [12], a multiphase level set framework for image segmentation using the Mumford-Shah model for piecewise smooth optimal approximations has been developed, which is the straightforward extension of their original work[2]. In [11], the authors also proposed a similar model that was able to segment images with intensity inhomogeneous. However, in reality,these models are difficult in implementation and computationally inefficient as discussed in[5]. More recently, local methods are used to deal with inhomogeneous images. A kernel function to define a local

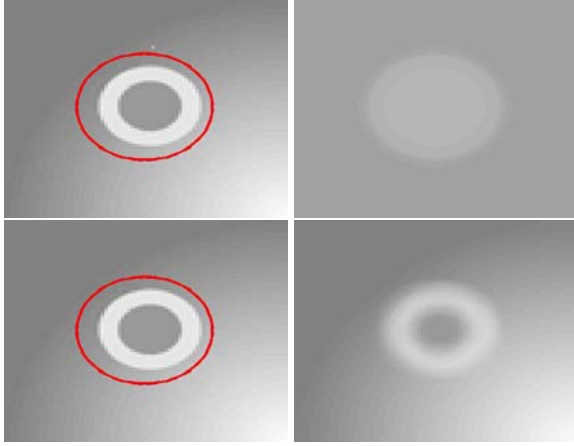


Figure 1. Comparison the solution images of the piecewise constant Mumford-Shah model and our model after initialization. Top: the result of piecewise constant Mumford-Shah model. Bottom: the result of our model

binary fitting energy in a variational formulation has been introduced[5]. In this model, the authors used a kernel function to control the size of the neighborhood, and the size of neighborhood are the same for all the pixels in the image. In [3], a nonparametric model for simultaneous image segmentation and smoothing based on local integration of the probability density functions has been proposed.

1.1. Contributions

Motivated by the idea proposed for edge-based segmentation[6], we realize that, for region-based active contours, more robust results can be achieved if the behavior of any individual point is constrained by both local image information of itself and that of its neighboring points. These inter-point relationships provide an expanded local view, and the global view in the extreme case when all the image points are considered, which becomes the same one as the Chan-Vese model[2].

This paper presents a novel region-based geometric deformable model that makes use of the image information at the support domain around each point of interest, thus effectively enlarges the capture range of each point to have a better regional understanding of the information within its local neighborhood. In other words, we establish the Mumford-Shah energy functional on each image point with its local neighborhood in a way such that it is capable of providing sufficient information to define a desired segmentation which is robust against intensity inhomogeneity and noise impact.



Figure 2. Left: Segmentation results with smaller influence domain—the image is segmented into two different objects, more fine details are preserved. Right: Segmentation results with larger influence domain—the image is smoothed heavily, and only one object is detected.

2. Methodology

2.1. The Mumford-Shah Functional

Let Ω be a bounded open subset of R^n , and $I_0 : \Omega \rightarrow R$ be an observed image. The behavior of the curve C subject to image information in Mumford-Shah formulation is dictated by:

$$F^{MS}(I, C) = \int_{\Omega} |I_0 - I|^2 dx + \lambda \int_{\Omega \setminus C} |\nabla I|^2 dx + \mu \cdot \text{length}(C) \quad (1)$$

The first term represents an image data-driven energy, which attracts the solution image I close to the observed image I_0 . The second term controls the smoothness of the solution image I , and the last term is the length of the evolving contour C . λ and μ are two positive parameters for controlling the weight of the two terms. The segmentation is done by minimizing the above energy functional and get the solution image I . However, it is not easy to minimize the above energy functional directly, since there has an unknown C , and also because the problems are not convex. In [2], Chan and Vese reduced the model into piecewise constant one, they assume that the solution image I are composed by two intensity piecewise constant regions, then the problem becomes a minimal partition problem. In this case, the second term of the above functional is eliminated. What's more, they solved the problem under the framework of level set[9], in which the contour C is replaced by the zero level set of a real-valued Lipschitz function ϕ : such that $C = \{x \in \Omega : \phi(x) = 0\}$. Inside the contour $\phi(x) < 0$, while outside the contour we have $\phi(x) > 0$

$$\begin{aligned}
F(\phi, C_1, C_2) &= \lambda_1 \int_{\Omega} |I_0(x) - C_1|^2 H(\phi(x)) dx \\
&+ \lambda_2 \int_{\Omega} |I_0(x) - C_2|^2 ((1 - H(\phi(x)))) dx \\
&+ \mu \int_{\Omega} \delta(\phi(x)) |\nabla \phi(x)| dx \quad (2)
\end{aligned}$$

where $\lambda_1, \lambda_2, \mu$ are fixed parameters. $H(\phi(x))$ is the Heaviside function, and $\delta(\phi(x))$ is Dirac function. C_1 and C_2 can be obtained through the first variation of equation (2) with respect to the constants C_1 and C_2 .

$$C_1(\phi) = \frac{\int_{\Omega} I_0(x) H(\phi(x)) dx}{\int_{\Omega} H(\phi(x)) dx} \quad (3)$$

$$C_2(\phi) = \frac{\int_{\Omega} I_0(x) (1 - H(\phi(x))) dx}{\int_{\Omega} (1 - H(\phi(x))) dx} \quad (4)$$

Please note that C_1 and C_2 are the global mean intensity of the region outside and inside the zero level set respectively. So the solution image can be expressed as

$$I = C_1 H(\phi) + C_2 (1 - H(\phi)) \quad (5)$$

The main drawback of this segmentation model is the potential existence of local minima in the energy functional. For example, proper segmentation often fails when regions are inhomogeneous or when regions are homogeneous but very noisy.

We argue from real world experiences that, more reliable and robust results can be achieved if image information from both the point itself and its neighboring points are properly included. It is clear that neighboring image information provides useful constraints and gives better regional understanding of the local boundaries.

2.2. Neighbor-Constrained Active Contours Without Edges

Originated from the piecewise constant Mumford-Shah model, the energy of an arbitrary point x in the image can be expressed as:

$$\begin{aligned}
E(x) &= |I_0(x) - C_1|^2 H(\phi(x)) \\
&+ |I_0(x) - C_2|^2 ((1 - H(\phi(x)))) \quad (6)
\end{aligned}$$

From the above energy we can see: if the point x is inside the evolving contour, its energy is the second term of the above functional, or its energy is the first term. However, all

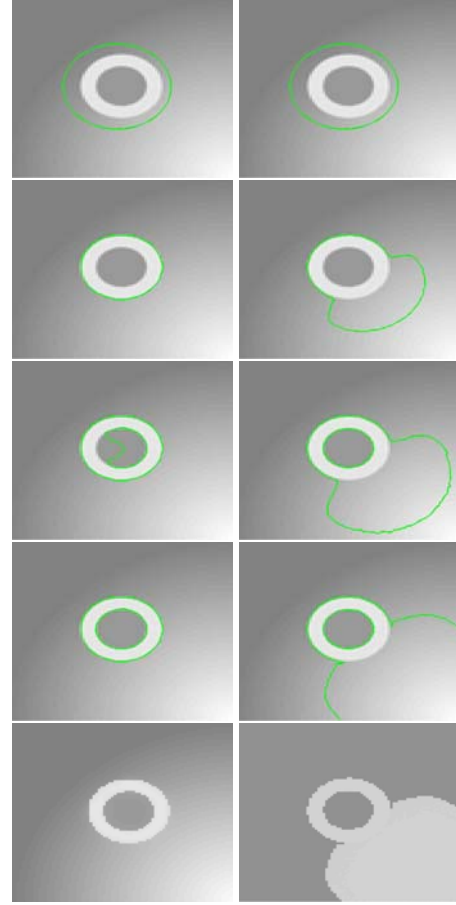


Figure 3. Comparison between our method (left) and traditional region-based method (right) on meeting images with intensity inhomogeneity—Our method converges properly using the neighborhood constraints, and the traditional one is affected by the intensity inhomogeneity.

the points inside the contour do not have the same intensity, neither do the points outside the contour. As a result, it is not accurate to just use two constant C_1 and C_2 to calculate the energy inside and outside the contour respectively. To improve the accuracy, we use the local mean intensity $I_1(x)$ and $I_2(x)$ instead.

Modifying the above original formulation by integrating over the *influence domain* $\Omega_e(x)$ (more details later) for each data point to incorporate the neighborhood influence, the following energy is achieved:

$$\begin{aligned}
E(x) &= \int_{\Omega_e(x)} |I_0(y) - I_1(x)|^2 H(\phi(y)) dy \\
&+ \int_{\Omega_e(x)} |I_0(y) - I_2(x)|^2 (1 - H(\phi(y))) dy \quad (7)
\end{aligned}$$

Here $I_1(x)$ is the mean intensity of all the points in the

intersection of inside the contour and the influence domain, and $I_2(x)$ is the mean intensity of all the points in the intersection of outside the contour and the influence domain. So $I_1(x)$ and $I_2(x)$ can be given by:

$$\begin{cases} I_1(x) = \text{average}(I_0) & \text{in } \Omega_e(x) \cap \Omega_{\text{inside}} \\ I_2(x) = \text{average}(I_0) & \text{in } \Omega_e(x) \cap \Omega_{\text{outside}} \end{cases} \quad (8)$$

$I_0(y)$ is the intensity of the point y within the influence domain of point x . Integrating over the whole image domain, we can reach the following energy functional:

$$\begin{aligned} & E(I_1, I_2, \phi) \\ &= \lambda_1 \int_{\Omega} \int_{\Omega_e(x)} |I_0(y) - I_1(x)|^2 H(\phi(y)) dy dx \\ &+ \lambda_2 \int_{\Omega} \int_{\Omega_e(x)} |I_0(y) - I_2(x)|^2 \\ & \quad (1 - H(\phi(y))) dy dx \end{aligned} \quad (9)$$

Here, λ_1 and λ_2 are two fixed positive parameters, to weight the energy inside and outside the contour respectively. In order to control the smoothness of the evolving contour, a full case of the above model is obtained by adding a term of the curve length:

$$\begin{aligned} & E(I_1, I_2, \phi(x)) \\ &= \lambda_1 \int_{\Omega} \int_{\Omega} \chi_{\Omega_e(x)}(y) |I_0(y) - I_1(x)|^2 H(\phi(y)) dy dx \\ &+ \lambda_2 \int_{\Omega} \int_{\Omega} \chi_{\Omega_e(x)}(y) |I_0(y) - I_2(x)|^2 \\ & \quad (1 - H(\phi(y))) dy dx \\ &+ \mu \int_{\Omega} \delta(\phi(x)) |\nabla \phi(x)| dx \end{aligned} \quad (10)$$

where $\mu > 0$ is a fixed parameter. $\chi_{\Omega_e(x)}(y)$ is the characteristic function of $\Omega_e(x)$, it equals to 1 when $y \in \Omega_e(x)$, and equals to 0 otherwise. As a result we can get the solution image, $I = I_1 H(\phi) + I_2(1 - H(\phi))$. If we minimize the above energy, it forces $I_1(x)$ and $I_2(x)$ to get closer to the intensity of all the points within its influence domain, which makes $I_1(x)$ and $I_2(x)$ be the mean intensity within the local domain. In Fig. 1, we can see two different solution images got from our model and the piecewise constant model. The left column is the observed image after initialization, and the right column are the solution images. The top row stands for the piecewise constant Mumford-Shah model, and the bottom row stands for our model. As we can see, the solution image on the bottom row is much closer to the observed image than the one on the top row. So we can get much better result than the piecewise constant

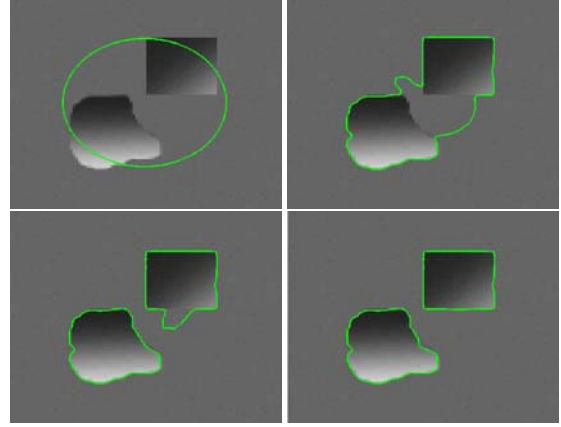


Figure 4. A segmentation result for an inhomogeneous image using our proposed method. The evolution process is listed with four figures from left to right, top to bottom. The parameters chosen for this example are: $\lambda_1 = 1, \lambda_2 = 1, \mu = 0.003 \times 255^2$.

Mumford-Shah model. In all, the function of the local integration are twofold: first, it makes the solution image be close to the original image; second, it smoothes the solution image.

2.3. Numerical Implementations

Now, let us take the first variation of the right hand side of Equation (10) with respect to I_1 and I_2 :

$$I_1(x) = \frac{\int_{\Omega} \chi_{\Omega_e(x)}(y) H(\phi(y)) I_0(\phi(y)) dy}{\int_{\Omega} \chi_{\Omega_e(x)}(y) H(\phi(y)) dy} \quad (11)$$

$$I_2(x) = \frac{\int_{\Omega} \chi_{\Omega_e(x)}(y) (1 - H(\phi(y))) I_0(\phi(y)) dy}{\int_{\Omega} \chi_{\Omega_e(x)}(y) (1 - H(\phi(y))) dy} \quad (12)$$

Note that $I_1(x)$ and $I_2(x)$ are the local mean intensity within the influence domain of the pixel x .

Finally, the following Euler-Lagrange Equation can be achieved by minimizing the whole energy with respect to ϕ :

$$\begin{aligned} \frac{\partial \phi}{\partial t} &= \delta_{\epsilon}(\phi) \left[-\lambda_1 \int_{\Omega} \chi_{\Omega_e(y)}(x) |I_0(x) - I_1(y)|^2 dy \right. \\ &+ \lambda_2 \int_{\Omega} \chi_{\Omega_e(y)}(x) |I_0(x) - I_2(y)|^2 dy \\ &+ \left. \mu \operatorname{div} \left(\frac{\nabla \phi}{|\nabla \phi|} \right) \right] \end{aligned} \quad (13)$$

In this paper, we set ϵ to be 1 and use the Heaviside function and Dirac function as in[2].

$$H_{\epsilon}(x) = \frac{1}{2} \left(1 + \frac{2}{\pi} \arctan \left(\frac{x}{\epsilon} \right) \right) \quad (14)$$

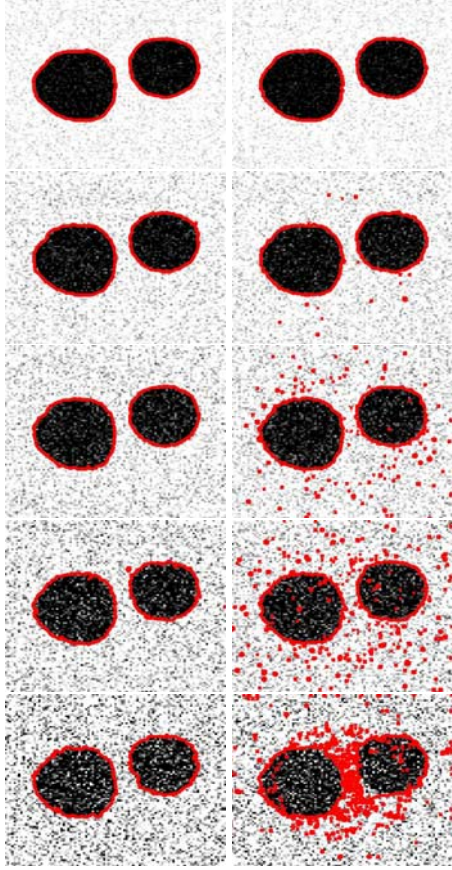


Figure 5. Comparison between traditional our algorithm (left) and region-based method (right) on noisy synthetic images.

Table 1. Comparison the accuracy of the proposed method with the piecewise constant Mumford-Shah model, where m_g is the ratio of number of pixels shared with the ground truth to the total pixels of the ground truth and m_e is the ratio of the number of the mismatch pixels to the total pixels in the segmentation.

Method	S/N(dB)	m_g	m_e
Our method	14.8	0.9939	0.0051
	10.2	0.9903	0.0142
	8.2	0.9856	0.0169
	5.8	0.9746	0.0243
	4.2	0.9698	0.0287
MS	14.8	0.9969	0.0127
	10.2	0.9901	0.0285
	8.2	0.9823	0.0525
	5.8	0.9703	0.1274
	4.2	0.9580	0.1959

$$\delta_\varepsilon(x) = \frac{1}{\pi} \left(\frac{\varepsilon}{\varepsilon^2 + x^2} \right) \quad (15)$$

To discretize the Equation (13), we use a finite differ-

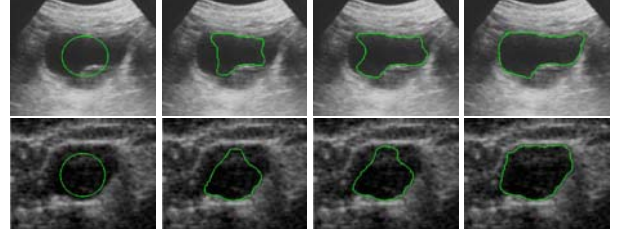


Figure 6. Segmentation of two ultrasound images using our method. The evolution process is listed with four figures from left to right. The parameters chosen for this example are: $\lambda_1 = 1$, $\lambda_2 = 2.4, \mu = 0.01 \times 255^2$ (top); $\lambda_1 = 1$, $\lambda_2 = 1.5$, $\mu = 0.08 \times 255^2$ (bottom).

ences implicit scheme:

$$\begin{aligned} & \frac{\phi^{n+1} - \phi^n}{\Delta t} \\ &= \delta_\varepsilon(\phi^n) \left[\mu \Delta_x^- \left(\frac{\Delta_x^+ \phi^n}{|\nabla \phi^n|} \right) + \mu \Delta_y^- \left(\frac{\Delta_y^+ \phi^n}{|\nabla \phi^n|} \right) \right] \\ & - \lambda_1 \int_{\Omega} \chi_{\Omega_e(y)}(x) |I_0(x) - I_1(y)|^2 dy \\ & + \lambda_2 \int_{\Omega} \chi_{\Omega_e(y)}(x) |I_0(x) - I_2(y)|^2 dy \quad (16) \end{aligned}$$

where $\Delta_x^- \phi_{i,j} = \phi_{i,j} - \phi_{i-1,j}$, $\Delta_x^+ \phi_{i,j} = \phi_{i+1,j} - \phi_{i,j}$, $\Delta_y^- \phi_{i,j} = \phi_{i,j} - \phi_{i,j-1}$, $\Delta_y^+ \phi_{i,j} = \phi_{i,j+1} - \phi_{i,j}$

$$|\nabla \phi^n| = \sqrt{(\Delta_x^+ \phi^n)^2 + (\Delta_y^+ \phi^n)^2}$$

2.4. Discussion

In practice, influence domains of different sizes generate different energy term, which in turn are suitable for different situations. For example, large influence domains are effective in robust segmentation of noisy images. On the other hand, small influence domains are needed for object boundaries with fine details. The segmentation results of a synthetic image with different influence domain size are shown in Fig.2 The left image is the result using small influence domain, the image is segmented into two different objects, more fine details are preserved. The right one is the result using large influence domain, the image is smoothed heavily, and only one object is detected. In this paper, the shape of the influence domain is a circle. However, using adaptive influence domain according to both the image data and the level set geometry may get a better result. Schemes to adaptively determine the sizes of the influence domains are undergoing.

3. Experiments and Results

We have conducted several experiments on synthetic and real images with our proposed method, and compared the

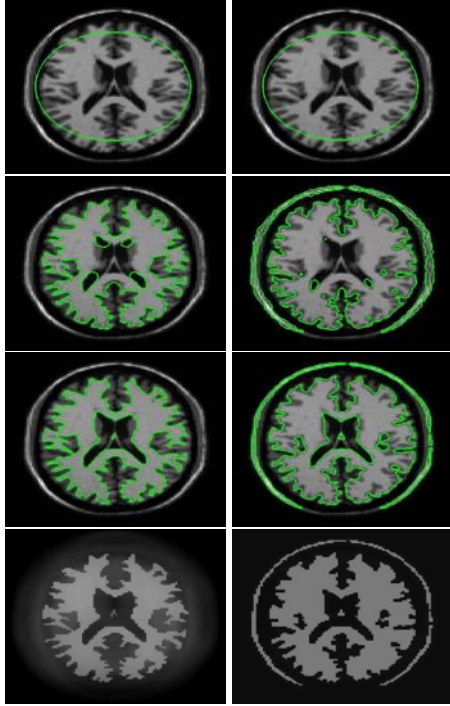


Figure 7. Application to white matter segmentation for MR images: the results of our method (left) and the segmentation result of the piecewise constant model (right). The evolution process is listed with four figures from top to bottom.

segmentation results with those from the traditional piecewise constant Mumford-Shah model.

In Fig.3, comparison is made between piecewise constant Mumford-Shah model and our algorithm on dealing with the inhomogeneous images. The first four columns are the progress of the evolution, and the last column is the solution image. As can be seen, our approach produces better segmentation results than the edgeless active contours scheme. Fig. 4 gives another example to segment images with intensity inhomogeneity when using proposed method in this paper. Implicit to traditional method is the assumption that each region, e.g., object and background, can be described by the mean gray level value. However, for the inhomogeneous images, such assumption is not true. Our proposed framework converges to the boundary since it has a better regional understanding of the information within its local neighborhood.

Next, we have performed comparative tests to examine our proposed method's tolerance to additive noises. Despite the fact that the images are noticeably worse, our method is still able to pick out the object boundary, as shown in Fig. 5. We treat the segmentation results of the clean image as the ground truth, then we define two values to measure the accuracy of the segmentation. The first one is the ratio of number of pixels shared with the ground truth to the total pixels

of the ground truth, denoting this value as m_g . The second one is the ratio of the number of the mismatch pixels to the total pixels in the segmentation, denoting it as m_e . The segmentation criteria is based on the notion that the larger m_g and smaller m_e , the better the segmentation results. As can be seen from Table. 1, the segmentation result obtained using our method is more accurate in comparison to that obtained by traditional edgeless active contours. The noise in image makes it difficult for piecewise constant Mumford-Shah model to achieve the real object boundary by using the global mean gray level value. Our method gives local understanding of the image and thus makes it more tolerable to noise.

In Fig. 6, we segment ultrasound images using our proposed method. As we see, neighbor-constrained edgeless active contour is less affected by local features. We have also tested the algorithms on brain images, as shown in Fig. 7. Application of the Chan-Vese algorithm resulted in a good segmentation, however with a large degree of noise(Fig. 7(right)). Clearly, our result yields a smooth boundary which captures the details more accurately. Finally, Fig. 8 shows the ability of our method to deal with nature image. The difficulty for segmenting this image is that part of head is more similar to the background. Once again, in this case, our proposed framework gives satisfactory segmentation results.

4. Conclusions

A novel region-based geometrical formulation for active contours, which combines local Mumford-Shah energy functional and the level set representation, is presented. We establish the Mumford-Shah energy functional on each image point with its local neighborhood in a way such that it is capable of providing sufficient information to define a desired segmentation which is robust against intensity inhomogeneity and noise impact. Experiments for different kinds of images are presented.

Acknowledgments

This work is supported in part by the National Basic Research Program of China (No: 2003CB716104), by the Natural Science Foundation of Zhejiang Province(No: R207119) and by the the National Natural Science Foundation of China(No: 60403040).

References

- [1] V. Caselles, R. Kimmel, and G. Sapiro. Geodesic active contours. *International Journal of Computer Vision*, 22:61–79, 1997.
- [2] T. Chan and A. Vese. Active contours without edges. *IEEE Transactions on Image Processing*, 10:266–276, 2001.

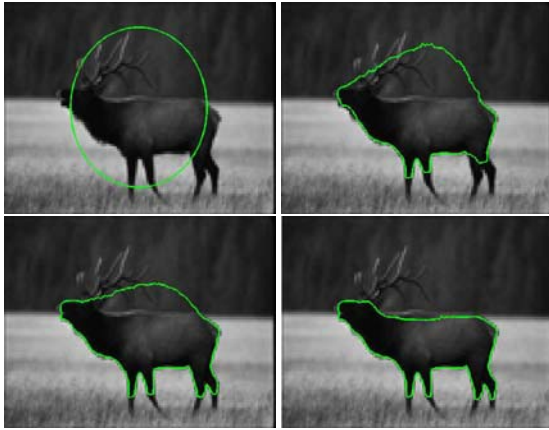


Figure 8. Application to a natural image. The evolution process is listed with four figures from left to right, top to bottom.

- [3] W. Guo and Y. Chen. using non-parametric kernel to segment and smooth images simultaneously. *Processings of International Conference in Image Processing*, pages 217–220, 2006.
- [4] M. Kass, A. Witkin, and D. Terzopoulos. Snakes: Active contour models. *International Journal of Computer Vision*, 1:321–331, 1987.
- [5] C. Li, C. Kao, J. C. Gore, and Z. Ding. Implicit active contour driven by local binary fitting energy. *Computer Vision and Pattern Recognition(CVPR)*, 1:1–7, 2007.
- [6] H. Liu, Y. Chen, W. Chen, and P. Shi. Neighborhood aided implicit active contours. *Computer Vision and Pattern Recognition(CVPR)*, 1:841–848, 2006.
- [7] R. Malladi, J. A. Sethian, and B. C. Vemuri. Shape modeling with front propagation: a level set approach. *IEEE Transactions on Pattern Analysis and Machine Intelligence*, 17:158–175, 1995.
- [8] D. Mumford and J. Shah. Optimal approximation by piecewise smooth functions and associated variational problems. *Commun. Pure Appl. Math*, 42:577–685, 1989.
- [9] S. Osher and J. Sethian. Fronts propagating with curvature-dependent speed: Algorithms based on hamilton-jacobi formulations. *Journal of Computational Physics*, 79:12–49, 1988.
- [10] N. Paragios and R. Deriche. Coupled geodesic active contour regions for image segmentation: A level set approach. *ECCV*, 2:224–240, 2000.
- [11] A. Tsai, A. Yezzi, and A. S. Willsky. Curve evolution implementation of the mumford-shah functional for image segmentation, denoising, interpolation, and magnification. *IEEE Transactions on Image Processing*, 10:1169–1186, 2001.
- [12] L. A. Vese and T. Chan. A multiphase level set framework for image segmentation using the mumford and shah model. *International Journal of Computer Vision*, 50:271–293, 2002.